Effect of solidification rate on pore connectivity of aluminium foams and its consequences on mechanical properties

J. Lázaro[1], E. Solórzano[1] and M.A. Rodríguez-Pérez[1], A.R. Kennedy[2]

[1] *Cellular Materials Laboratory (CellMat), Condensed Matter Physics Department, Science Faculty, University of Valladolid, Paseo de Belén 7, 47011 Valladolid, Spain*

[2] *Manufacturing Research Group, Faculty of Engineering, University of Nottingham, University Park, NG7 2RD Nottingham, UK*

Corresponding author: Jaime Lazaro

Email: jlazaro@fmc.uva.es Telephone: +34 98342 3572 Fax: +34 98342 3192

Abstract

This study evaluates the influence of solidification rate on the generation and control of pore connectivity of closed-cell aluminium foams. Additionally, it gives the experimental support to evaluate and model the effect of this pore connectivity on the mechanical properties. A collection of AlSi10 foams produced via powder metallurgy route, with porosities between 0.65 and 0.85, were examined. During production, applied heating conditions were the same in all cases but the cooling conditions were varied in order to promote different solidification rates in a wide range (from -1 to -15 K/s). Structural characterization was performed by gas pycnometry and X-ray microtomography while the mechanical properties were evaluated by microhardness measurements and uniaxial compression tests. Results showed a clear reduction of pore connectivity when increasing the solidification rate. The consequence is a prominent improvement of the foam strength over the one expected from just the matrix refinement. Further analysis on this relationship between the pore connectivity and the mechanical properties, has allowed to propose a correction to the theoretical model for collapse strength in closed cell foams to consider such contribution and predict more accurate results.

Key words: aluminium foam; solidification; pore connectivity; mechanical properties; modelling.

1. Introduction

Despite the apparent closed cell structure of aluminium foams [1], it is well known that their mechanical response is below those values predicted by models for closed cell cellular materials [2-4]. In addition, these materials exhibit a high scattering in mechanical properties in comparison with other cellular materials [5-7], something that limits their potential use in structural and load-bearing applications, even when they are used as cores in sandwich structures [8-11]. The scattering in properties is typically explained in terms of irregularities in pore morphology (size, shape, anisotropy, cell wall corrugations and curvatures, etc. [12]) or density inhomogeneities [13], derived from a non-optimum control of the initial nucleation and later evolution of the material.

Besides the variability, the poor mechanical performance of aluminium foams also depends on other structural defects such as missing and/or partially broken cell walls, which have already been reported in previous studies as initiation points for mechanical failure [5, 14-16]. These defects are also call interconnections (absence of a cell wall between two adjacent pores) and denoted as pore connectivity or open cell content when referring to the global structure.

However, it is surprising how the effect of this characteristic is not taken into account in the model of strength for closed-cell materials [2, 3] when, in fact, its presence could explain itself why the strength of aluminium foams tends to fit better to the predictions for open cell cellular solids. Actually, the model considers the foam as a regular entity with flat cell walls and even typical corrugations and curvatures have to be considered separately to achieve a more realistic prediction [12], as will be discuss later on the paper.

Furthermore, the importance of interconnections is not limited to the mechanical properties. They also play a key role in other physical properties and related functional applications dealing with fluidsas buoyancy (ship building [17]), permeability (fluids

penetration and filtration), acoustic control [18-20], efficacy of heat treatments [21]) and thermal transport (isolation, heat exchange [22] and fire resistance [23], among others.

Therefore, there is a clear necessity to understand cell wall cracking mechanisms and their effect on properties in order to be able to improve and/or control the cellular structure of these materials. In the same way, it is necessary to develop better models to take into account this type of defect and so predict the properties with more accuracy.

Despite the aforementioned expected relevance of pore connectivity, there is scarce information in the literature about this type of defect. Regarding structural characterization, McCullough et al. [24] succinctly mentioned that approximately a third of the cell faces in foams produced by the powder metallurgy (PM) route present hairline cracks. Elmouataouakkil et al. [25] found, by X-ray tomography analysis, a pore connectivity in PM foams near to 50% in 2D slices and 100% in 3D analysis, while no connectivity was reported on foams produced by direct melt foaming. A later study by Solórzano et. al. in 2008 [26] employed air pycnometry to provided further characterization of this defect over a collection of foams of dissimilar density and manufactured by different routes. Results were in agreement with previous findings and highlighted the particularly high pore connectivity of PM foams in comparison with the other types obtained by melt route.

Causes of rupture and crack generation have also been studied. Most of these studies have been based on the PM route, mainly because of the easy to produce samples under different conditions and the possibility to control the production parameters and analyse them individually [27]. It is assumed that the final observable cracks (interconnections) are generated during the solidification step and thus, studies involving in-situ characterization were first proposed. Stanzick et al. [28] validated the effectiveness of X-ray radioscopy for estimating the number, the rate and the distribution of cell wall ruptures, in particular during the solidification step. Further investigation of the solidification step by radioscopy was

performed by Mukherjee et al. [29]. They found that, under certain conditions, the solidifying foam exhibits an unexpected small expansion and simultaneously the alloy suffers intrinsic solidification shrinkage [30]. Recent studies of this phenomenon (denoted by Mukherjee et al. as *solidification expansion* or *SE* [31]) have shown that it is directly correlated to the amount of cell wall ruptures during solidification [32] and therefore, it is thought to be one of the reasons for the presence of cracks in the final solid structure. Further investigations revealed that the extent of solidification ruptures depends significantly on the alloy composition (via different H_2 precipitation and solidification shrinkage) [33], on the total foaming time (via remaining blowing agent) [31] and, more particularly, on the cooling rate [34, 35].

Nonetheless, complete control of pore connectivity during foam production and a good understanding of the structure-properties relationship are still lacking. Accordingly, one of main objectives of the present study has been to analyse both aspects. To this end, the effect of cooling conditions on pore connectivity generation has been evaluated for aluminium foams with different densities. The characterization of the cellular structure has been performed in parallel by both gas pycnometry and X-ray tomography analysis. Furthermore, the effect of pore connectivity on the mechanical response has also been analysed, modelled and discussed, contributing an advanced model which includes the cell connectivity to predict more accurately the values of collapse strength in metal foams.

2. Experimental

2.1. Materials

The foams studied in this work were fabricated, via a PM route [27], by using a precursor material supplied by Alulight Company (Ranshofen, Austria). It consisted of a group of Extruded-Strips (E-S) with a cross-section of5 mm x 20 mm, which had been produced via the direct powder extrusion (Conform) method [36]. The composition of this

precursor material was based on a mixture of Al (90 wt.%) and Si (10 wt.%) elemental powders and contained 0.8 wt.% of untreated TiH_2 powder as a foaming agent.

2.2. Foam preparation

The foaming process was conducted using machined stainless steel moulds (2.5 mm in thickness) with a cylindrical geometry. This mould shape was selected to ensure homogeneous foaming conditions (heating and cooling) and reproducible cellular structures. Moulds used had a height of 36 mm and an internal diameter of 17 mm. Therefore, all foams produced had an external volume of 8.17 cm^3.

To produce the foam specimens, cut pieces of precursor strips, with a mass according to the desired density, were placed in the mould and then the mould was closed and introduced inside a pre-heated furnace at 650ºC. This heating ensured the complete melting of the solid precursor pieces and their later expansion (foaming) due to the hydrogen gas release during the thermal decomposition of the TiH_2 (TiH_2 (s) + heat → Ti (s) + H_2 (gas) [1]). The mould was taken out from the furnace after the expanded liquid-gas structure (foam) had completely filled the mould, a period which typically varies between 13 and 20 minutes [37]. The stabilization of the liquid foam (solidification) was affected using three different cooling conditions: (i) blowing homogeneously the mould with compressed air at low pressure (1bar); (ii) blowing homogeneously the mould with compressed air at higher pressure (6bar); (iii) introducing the entire mould into water at room temperature (~25ºC).

In order to ensure the reproducibility of the results and reduce the statistical variations at least three samples were fabricated for each density range considered and for each type of cooling applied. In total, more than 60 foams with porosities ranging between 0.65 and 0.85 (thus relative densities between 0.35 and 0.15) were produced.

In addition, complementary foaming tests were performed with the objective of measuring the temperature evolution inside the foam during the cooling process and to determine the solidification rate corresponding to the different cooling conditions. To this end, a hole was drilled on the upper mould lid and Swagelok™ fittings (refs. ss-102-1, ss-103-1, ss-104-1) were screwed onto it, similarly to the method used in previous work [21]. This special sealing system avoids water penetration, something that could distort the temperature measurement and/or damage the foam structure. Additional high temperature seals were placed in between the lids and the mould, in order to prevent water penetration during quenching, and the lids were tightened with screws. A K-type thermocouple (1.5 mm diameter) was introduced through the Swagelok™ connector, placing the thermocouple's tip at the centre of the foam, as shown in figure 1. At least three foaming tests were performed for each type of cooling, registering the temperature evolution versus time.

2.3. Structural characterization

The characterization of the cellular structure has been focused mainly on the cracks or interconnections present in the cell walls, a type of defect that is expected to have a notable influence on the mechanical behaviour [2]. To this end, two non-destructive techniques were employed: the gas pycnometry technique and X-ray computed tomography analysis.

It is important to mention that the outer skin of the examined foamed parts was not removed for this characterization. The main reason for keeping it is because the external, intrinsic, skin is one of the best/main characteristics of foams produced by the PM route and it is generally present in components based on this material [35]. In regard to the results obtained, it can be interpreted that this skin is not completely dense, containing defects [37] and open porosity that connects the interior of the foam with the atmosphere. Therefore, it is convenient to consider these imperfections in the evaluation of the structural quality and the

derived properties of the entire foamed part. Nonetheless, later studies in previously tested samples after skin removal did not yield significant differences in the analysed characteristics.

2.3.1. Gas pycnometry

All foams produced in this work were characterised by the gas pycnometry method. This technique is very similar to air pycnometry, which has already been reported as a fast and effective tool to evaluate and quantify the pore connectivity in aluminium foams [26,33,38]. Gas pycnometry is, actually, more precise than air pycnometry although there is no significant difference in the case of the "large" air volumes determined in foamed materials. The method itself determines the apparent volume of the sample, i.e. the fraction of isolated gas plus the solid fraction in the foam. The fraction of gas inside the sample that is connected to the exterior is not considered, but can be calculated by comparison with the external geometric volume, thus being an indirect indicator of the open cell content of the foam.

Characterization by using this technique was conducted under the ASTM standard D6226-05 [39] using an Accupic 1330 (Micromeritics®) gas pycnometer, working with helium as a filling gas. According to this standard, the open cell content (C_{open}) is calculated using expression (1). In this expression, V_{sample} is the external geometric volume of the foam, V_{pyc} is the volume measured with the pycnometer and p is the porosity, i.e. the total volume fraction of air contained in the sample. Note that V_{sample} has to be calculated from the external dimensions of the specimen, so regular shapes (cylindrical and/or prismatic samples) are recommended. From the expression, it can be observed that the value of C_{open} is always between 1 (100% open cell content) and 0.

$$C_{open} = \frac{V_{sample} - V_{pyc}}{V_{sample} \cdot p} \quad (1)$$

2.3.2. X-ray computed microtomography (μCT)

Foams of similar density obtained under different cooling conditions were selected to evaluate their 3D cellular structure by μCT. The measurements were performed using a Skyscan μCT system (mod. 1174) [40], with a final voxel size of 20 μm^3 in all cases. Subsequent 3D reconstruction of the data was performed using the commercial software *Octopus* [41]. After 3D reconstruction, Morpho+ software [42] was used to analyse the data and obtain numerical information about the cellular structure and its defects.

2.4 Mechanical characterization

The mechanical response of the foams is a combination of the matrix strength and the response of the cellular structure [2]. For that reason, the characterization was focused foam matrix by using microhardness measurements (section 2.4.1) and the response of the foam (matrix + cellular structure) by uniaxial compression tests (section 2.4.2).

2.4.1. Microhardness measurements

Selected samples with similar density subjected to each type of cooling were used to evaluate the effect of solidification rate on the foam matrix microstructure. Vickers Microhardness (HV) was measured along a radial profile at the mid-height of the foam.

To this end, 3 mm slices were cut at the mid-height of the samples and infiltrated with epoxy resin (Specifix 20, Struers®, Ballerup, Denmark) using a vacuum system (Epovac, Struers) to ensure complete filling of the cut pores with the resin. The embedded specimens were ground and polished. Concentric circles were drawn on the polished surfaces with the objective of defining radial regions in which the indentations were to be made. This methodology was tested with success in a previous study [21].

A Carl Zeiss microhardness tester, mod. MHO IB (West Germany), was used to perform the Vickers Microhardness (HV) measurements. All the indentations were made using a load of 20g for 15s (HV 0.02/15) following the testing standards [43], ensuring sufficient distance (at least three times the indent size) from one indentation to another and a similar distance from the edge of the cell wall. To compensate for the typical scatter associated with this kind of measurement, at least five indentations were made in each region.

2.4.2. Uniaxial compression tests

Prior to carrying out the compression testing experiments, samples were cut into two pieces. Thus, new samples (17 mm in diameter, 18 mm in height) with dimensions within the standard testing procedure guidelines [44] were obtained. The cutting process exposed some pores in one of the planar faces to the atmosphere and this change in contribution to the open cell content needed to be corrected. Therefore, the density and the open cell content, applying the correction method included in the ASTM standard [39], were measured again. However, no significant differences were observed in both ρ and C_{open} for the specimens when comparing the values before and after the cutting process (differences < 5% in all cases).

Quasi-static uniaxial compression tests were carried out on an Instron (mod. 5.500R6025) universal materials testing machine, at 23 ºC, at a displacement rate of 1.8 mm min^{-1} (strain rate of $1.67 \cdot 10^{-3}$ s^{-1}) up to a nominal strain of 75%.

3. Results and discussion

3.1. Temperature evolution during the cooling process

The determination of the internal temperature of aluminium foams during the foaming process has been accomplished by other researchers in expandometry and X-ray radioscopy tests as well as inside moulds [45, 46], although these types of measurements have associated

methodological complexities. Figure 2 represents temperature evolution at the central position in foams with a similar density when both foam and mould are exposed to the three different cooling conditions considered. It can be observed that temperature evolution is clearly different for the three foams. As expected, the sample cooled using water cools down to room temperature very quickly, while complete cooling with pressurized air takes much longer times.

The solidification rate (V_{sol}) has been calculated in the region between solidus (~577 ºC) and liquidus (~597 ºC) temperatures (marked with horizontal lines in figure 2). Table 1 (column 2) presents the average values after analysing three temperature records for each type of foam of similar density. From the values obtained, it can be appreciated that when using compressed air, the solidification rate at the centre ranges between 0.5 to 2 K/s, significantly influenced by the pressure of the air. However, when using water as cooling medium, the solidification rate increases considerably, approximately by one order of magnitude. Thus foams cooled by water quenching can solidify completely in less than 2 s. The results presented here, both for air and water quenched samples, are in good concordance with previous measurements reported in the literature (V_{sol_air} ~ 1 to 3 K/s [31] and V_{sol_water} > 10K/s [35]. It should be kept in mind that the values obtained in this study correspond only to the central part of the foams and much higher rates are expected in other parts of the foam close to the mould. In case of necessity in future investigations, additional thermocouples at different points inside the foam could be used, or even alternative techniques based on finite element simulation could be applied to solve the temperature evolution equation within the complete foam volume, as has been already proposed by the authors in previous studies [21, 47].

3.2. Foam structure

The evaluation of the cellular structure characteristics has been divided into three parts, from the macro to the micro scale and evaluating changes induced by the different cooling conditions. Macroscopic pore connectivity, characterized by gas pycnometry, is shown in section 3.2.1. The main structural parameters are evaluated in section 3.2.2. Finally, a description of the size and distribution of the interconnections inside the foams is provided in section 3.2.3.

3.2.1. Effect of solidification rate on open cell content

The results obtained by gas pycnometry are shown in figure 3. The points displayed in the graph represent the average values for the open cell content (C_{open}), with the corresponding standard deviation (error bars), for foams of similar porosity. The trend curves (dashed lines) for each type of cooling have also been included to allow for a better visualization of the dependence with porosity.

It can be appreciated that, independently of the cooling method, the open cell content of the foams increases with the sample porosity in the analysed range. A similar trend has already been reported by the authors in previous works [26, 33] and it is associated with the reduction in foam stability with increasing porosity during solidification. If it is assumed that that cell wall thickness decreases with sample density [2], then it seems reasonable that the probability of wall/film rupture or crack generation during solidification shrinkage will tend to increase as the sample porosity increases. In addition, the higher the porosity, the lower the thermal conductivity (and diffusivity) of the foam, thus promoting slower cooling and the associated defects.

The slope for the trend of C_{open} with porosity in the analysed range seems similar for the three different types of cooling studied. This makes sense considering that the samples are

based on the same alloy and foamed under the same conditions. It has been found by the authors that for different powder compaction techniques (e.g. PM foam precursors) or another alloy compositions, a different slope in the $C_{open}(p)$ trend is observed [33].

Nevertheless, the most important result is the large difference between foams cooled by air ($C_{open\_air} > 60\%$) and those cooled with water ($C_{open\_water} < 40\%$). The average values for C_{open}, within the whole porosity range, are presented in table 1 (column 3). Comparing the three types of cooling, it can be observed that the highest values of C_{open}, all over 80%, correspond to the foams solidified with compressed air at 1bar. These specimens are the ones with the slowest cooling rate. Connectivity values for foams solidified by fast air blowing (6bar) vary principally between 60 to 85 % while, finally, samples solidified with water, at a much higher rate, show C_{open} values in the range 10 to 40 %. Therefore, it is clear that the increase in solidification rate when cooling has a marked effect on pore connectivity. The mechanisms causing this reduction on connectivity with increasing cooling rate are discussed elsewhere [32, 33], which are fundamentally based on the hydrogen precipitation during solidification and/or the hydrogen released by the remaining blowing agent. These mechanisms are affecting the *solidification expansion* [31], mentioned in the introduction. In this sense, the faster the cooling step is, the lower will be the possible effect of *solidification expansion* on the generation of cell wall ruptures during solidification.

3.2.2. Effect of solidification rate on cellular structure

Microtomographic images enable further evaluation of the foam structure. Figure 4 shows the internal aspect, at the mid-height of each sample (h ~ 18 mm from the bottom), of three representative foams of similar porosity (p ~ 0.76). The particular open cell content (C_{open}, figure 3) for these samples is 95% for the foam solidified with air at 1 bar (figure 4a),

80% for the foam solidified with air at higher pressure (figure 4b) and 14% for the sample solidified by water quenching (figure 4c). .

From the slices in figure 4 it is apparent that the three foams exhibit a similar aspect in terms of the material distribution despite the notable differences in their open cell content. The specimens present a cylindrical symmetry and the material is distributed with a certain gradient in the radial direction from the centre to the lateral skin as already reported elsewhere [21, 48]. The three foams exhibit higher density (smaller pores) near the outer region and lower density (larger pores) in the central region. The vertical density distribution (shown in figure 5) does not show significant differences, which is expected for similar foam evolution during foaming (heating) under same conditions. Porosity profiles are nearly constant in the inner part and decrease (higher density) near the top and bottom basis of the foam near the skin. The constant density denotes the stability of these foams during the liquid stage before solidification with no evident drainage.

Despite the similarities in the material distribution inside the foams, the differences in terms of presence of defects are visible. Samples cooled in air exhibit a higher amount of missing or broken cell walls (marked with arrows in figure 4) in comparison with the sample cooled with water. In addition, the location of this type of defect correlates with the zones of lower density, i.e. the centre or near the larger pores. A more complete discussion of this difference in the amount and the location of defects is provided in the next section.

The structure has also been analysed in terms of pore size and pore sphericity in order to evaluate the possible influence of the cooling rate on these two structural parameters. To this end, the tomographs were filtered (median 3D, 2 pixels) and binarized, trying to fix a threshold high enough to avoid missing the existing cell walls in this process. A watershed algorithm was then applied in order to identify and separate the interconnected pores. The obtained images were revised and manual corrected, so eliminating those possible wrongly-

identified pore interconnections. The separating walls "artificially" created by the watershed algorithm represent the existing interconnections within the specimens and will be analysed in the next section.

More than 6000 pores were identified in each specimen, enough for providing a meaningful statistical analysis. The pore size was calculated as the equivalent diameter (Φ) of a sphere with the same pore volume ($V_{pore} = \pi\Phi^3/6$), whereas the sphericity was defined as the ratio of the external surface of a sphere with the same volume, divided by the 'real' pore surface computed in the 3D image analysis (A_{pore}). In other words, pore sphericity (Ψ_{pore}) has been calculated using expression 2. Figure 6 shows the pore size (figure 6a) and pore sphericity (figure 6b) histograms. The mean values for each structural parameter (Φ_{mean}, Ψ_{mean}) were obtained after fitting the histograms shown in figure 6 to normal functions ($R^2 > 0.85$ in all cases).

$$\Psi_{pore} = \frac{\pi^{1/3}(6V_{pore})^{2/3}}{A_{pore}} \qquad (2)$$

Φ_{mean},= 1300 ± 25 μm and Ψ_{mean} = 0.77 ± 0.08 was obtained for sample solidified by slow air blowing, whereas Φ_{mean},= 1259 ± 29 μm and Ψ_{mean} = 0.78 ± 0.07 was obtained for sample solidified by fast air blowing and Φ_{mean},= 1329 ± 24 μm and Ψ_{mean} = 0.76 ± 0.09 for the foam solidified by water quenching. It can be therefore appreciated that these three specimens are very similar in terms of pore size and pore sphericity. The only difference is observed in the samples cooled with air, which present a higher fraction of pores larger than 2500 microns. Therefore it should be noted that conventional analysis by tomography does not reveal significant differences, indentifying the need for more detailed 3D analysis of the identified interconnections.

3.2.3. Effect of solidification rate on pore interconnections

The pore interconnections were identified by subtracting the original binarized images from those including the "artificial" cell walls created by the watershed algorithm. The results, in the form of 3D renderings, are shown in figure 7a for the foam cooled with compressed air at 1 bar, the specimen with the highest C_{open} (95%), and in figure 7b for the water-quenched foam, with the lowest C_{open} (14%). Table 1 (columns 4 to 7) includes the statistical information about the number of pores identified in each foam, the number of interconnections detected, their mean size (average of *Feret's diameters* as described later) and the total volume they 'occupy' inside the structure.

It can be clearly seen that the air-cooled specimen presents much more interconnections in comparison with the one solidified with water (around 3 times), meanwhile the number of interconnections is very similar for both samples cooled with air. In addition, it can be appreciated that the interconnections are in both case concentrated in the central region, the region with the slowest cooling rate. Nevertheless, the air-cooled foam (figure 7a) also shows a high fraction of interconnections (~40%) in regions close to the outer skin, whereas only a few are observable in that region in the sample cooled in water (figure 7b), probably because the fast solidification. The size of interconnections located at the central region is higher while those located closer to the outer skin are smaller. All these observations can be associated with the local pore size and porosity since the central region exhibits larger bubbles and higher porosity while the opposite can be found near the outer skin.

Figure 8 shows the interconnection size distribution for the three analyzed specimens. In this particular case the flatness of these entities needed to be taken into account. Therefore, the selected parameter to describe the size of the interconnections was the *Feret's diameter* (in the plane of the 'reconstructed' interconnection), since the use of the equivalent diameter as shape descriptor would lead to unrealistic size analysis. The mode value of the three

distributions is located at approximately 140 μm, which means that large fraction of the population of the interconnections present in foams are of a small size. This could be also an effect of the resolution combined with the binarization threshold. Comparison of the three distributions shows that a reduction in the solidification rate tends to increase the size of the interconnections (see mean size in table 1, column 5). It is difficult to find interconnections larger than 500 μm in the water-quenched sample while a significant number of large interconnections (> 500 μm) are observed in the air-cooled samples. This fact, together with the corresponding number of interconnections in each foam, makes the total volume the interconnections represent or 'occupy' inside the foam to be much smaller in the case of the foam solidified with water in comparison with the samples solidified with air at high or low pressure (4 to 7 times smaller respectively; see table 1, column 6) which is clearly in agreement with the distribution of interconnections shown in figure 7.

3.3. Mechanical properties

Results in this section are divided in three parts. The first two parts correspond to the analysis of the matrix strength (section 3.3.1) and the foam strength (section 3.3.2) in terms of the different cooling conditions evaluated. The last part (section 3.3.3) is dedicated to analysis of the influence of defects (interconnections) on the foam strength, once the matrix contribution has been normalized.

3.3.1. Effect of solidification rate on matrix strength

It is well known that the solidification rate has a large influence on the microstructure of metals. Particularly, high cooling rates will reduce the grain size [49] and influence the morphology of the secondary phases (Si in this case) [50]. Obviously, these effects have also been observed in aluminium foams [31, 35]. Since the grain size and matrix strength (σ_y) are related by the *Hall-Petch* relationship [51], it follows that increases in solidification rate will

result an increase in matrix strength. In this study, Vickers microhardness (*H*) measurements have been used to quantify this effect through the relationship in expression 3 [52].

$$\sigma_y \approx H \ / 0.3 \tag{3}$$

Figure 9 shows Vickers microhardness profiles (in the radial direction) for three foams with similar porosity (p ~ 0.76), each one representative of the different cooling conditions analysed. From the data collected and the trends (dashed lines), it seems that the local hardness depends on the radial position, with higher values nearer the outer skin. This result is very similar for all three cases and probably corresponds with the variation of local solidification rate at different radial points, with lower rates in the central zone and thus reduced local strength. Nonetheless, the measurement fluctuations are also comparable with the experimental measurement error in this type of test (up to 10%) and it can be assumed that, in general, the three samples exhibit a reasonably uniform matrix microstructure along the radial direction and that the small gradient in hardness will not significantly affect the global mechanical response of the foams.

The comparison of hardness profiles for the three cooling conditions applied shows more interesting results. The average hardness values along the radial profile have been calculated and the results are shown in table 1 (column 7), together with the calculated yield strength of the matrix (σ_y) according to expression 3 (table 1, column 8). Foams solidified with compressed air at 1 bar (low cooling rate) exhibit the lowest strength, followed by those of foams cooled down with air at 6 bar. Nevertheless, the increment when cooling with air at 6 bar is relatively small (< 5%), similar to the measurement fluctuations. However, the foams cooled down by water quenching exhibit significantly higher values. In particular, the average hardness of water-quenched foams increases around 14% when compared with fast air-cooled foams (6bar) and around 19% when compared with slow air-cooled specimens (1bar). As expected, this hardening is consistent with the increase in the solidification rate (table 1,

column 2). Examination of other specimens with different porosity levels showed no significant variation in hardness values and trends. Thus, we can consider these values (table 1, column 7) to be independent of porosity.

3.3.2. Effect of solidification rate on foam strength

Figure 10 presents the stress-strain curves for the three representative foams shown in figure 4. Each one corresponds to the average response of the two parts obtained from each foam specimen (see section 2.4.2). It should be mentioned that the difference in the mechanical response of these two parts (top and bottom) for each sample was very small, in agreement with the high homogeneity in the vertical density profile (see figure 5).

As can be observed in figure 10, the three foams exhibit ductile deformation, with the highest response corresponding to the water-quenched sample, followed by those for the air-cooled samples, which exhibit quite similar behaviour. The typical stress peak after the elastic region (first local max., marked with an arrow in figure 10) has been used to define the *collapse strength* value (σ_c) of the foams.

The smallest value of σ_c (10.3 MPa) corresponds to the sample solidified by blowing with air at low pressure (1 bar). The sample cooled faster by using compressed air at 6 bar presents a higher value of σ_c, 11.9 MPa, i.e. an increment of around 15%. A much higher collapse strength is registered for the foam quenched in water, σ_c = 17.1 MPa. This value represents increments of +43% and +65% when compared with the samples cooled by air at 6 bar and 1 bar respectively. These differences in foam collapse strength are much higher than the equivalent variation in the matrix hardness (table 1, column 7) and the associated matrix strength according to expression 3. It is expected, therefore, that an additional contribution to the strength comes from the cellular structure, particularly from the dissimilar amounts of defects such as pore interconnections (figures 3, 7 and 8), since the main structural

parameters, i.e. density distribution, pore size and pore shape, are very similar for these three samples (figures 4, 5 and 6).

3.3.3. Effect of open cell content on foam strength

Figure 11 shows the variation in the normalized collapse strength ($\sigma_c^* = \sigma_c/\sigma_y$, where σ_y correspond to values shown in table 1, column 8) as a function of the foam relative density (ρ_r). Each point (symbol) in the figure represents the average value of σ_c^* for tested specimens with similar ρ_r and also similar C_{open}. The standard deviation (error bars) is similar in all cases (< 5%) and thus it has not been included, allowing a better appreciation of the results. Normalization of collapse strength "corrects" the dissimilar matrix strength and allows for a clearer comparison between the three types of samples in terms of their different cellular structure alone. After this normalization it can be appreciated that the collapse strength (σ_c^*) of the water-quenched foams is higher than the corresponding value for foams cooled with air. In particular, the samples cooled with air at 1bar exhibit the lowest values. It can, therefore, be concluded that an increase in the solidification rate after foaming significantly increases the mechanical response of the foams, independently of the relative density.

Figure 11 also includes the values of σ_c^* predicted by the theoretical models proposed by Gibson and Ashby [2] for open cell and closed cell materials up to a relative density around 0.3. The analytical functions describing both curves are given in expression 4 and expression 5 for open and closed cell materials respectively. In these models, the term with the exponent n = 3/2, represents the mechanical resistance of the Plateau borders and the edges, while the linear term represents the contribution of the cell walls to the global strength and thus, it is only present in expression 5 (closed cell model). K_1, K_2 and K_3 are coefficients related to the cellular structure, particularly to the solid distribution within the walls and the

edges. The accepted values for these coefficients, obtained from empirical comparison with experimental data, or by simulation, are K_1 = 0.3 for the open cell model [2] and K_2 = 0.33 and K_3 = 0.44 for the closed cell model [13], and therefore these have been the values used in this paper for the lines plotted in figure 11.

$$\sigma_C^{*\,OC} = K_1 \cdot (\rho_r)^{3/2} \tag{4}$$

$$\sigma_C^{*\,CC} = K_2 \cdot (\rho_r)^{3/2} + K_3 \cdot (\rho_r) \tag{5}$$

It can be appreciated that the experimental collapse strength is in all cases between the two main theoretical predictions, although data tend toward the closed cell model at high relative densities and are nearer the open cell model as the density decreases. It should be mentioned that the theoretical model for the closed cell materials (expression 5) is based on the assumption of unrealistic 'ideal' cellular structures with flat cell walls. Figure 4 clearly shows that these foams typically exhibit curved cell walls and corrugations that will have a detrimental effect on the mechanical response.

The effect of cell wall curvature and corrugations on the collapse strength of aluminium foams has been already studied by Simone and Gibson using a finite element method over a varied group of modified 'ideal' cellular structures [12]. They found that the contribution of both types of defect depends strongly on the foam density (via the cell wall thickness) and that the contribution from curvature is in general much higher than the contribution from corrugations. The effect of corrugations was only found to be of significance in low density foams (ρ_r < 0.1), when the wall thickness is of the same scale as the amplitude of the corrugations. It was suggested that the effect of curvature on the collapse strength could be easily addressed by introducing a correction factor ($f_{curvature}$) as it appears in expression 6. The factor $f_{curvature}$ is 1 for an ideal closed cell foam with flat cell walls and decreases with foam porosity (density reduction) and, obviously, with the increase of wall curvature [12]. A similar

approach could be taken to take into account corrugation effects in low density foams (ρ_r < 0.1).

$$\sigma_C^{*\,curvature} = \sigma_C^{*\,CC} f_{curvature} \tag{6}$$

Further characterization by Andrews et. al [53] and Sanders [54], of diverse, commercially available, metal foams, showed that Alulight-type foams generally exhibit a significant cell wall curvature (defined as the ratio of cell chord length to diameter, *L/2R*, for an equivalent spherical cap), between 0.1 and 0.7, with an average value around *L/2R* ~ 0.4. According to their discussions and findings [53], as the collapse strength is mainly controlled by the weakest region inside the foam, the 95th percentile within the cell wall curvature distribution should be used as the reference value to estimate the reduction in $\sigma_c^{*\,CC}$ ($f_{curvature}$) as proposed by Simone and Gibson [12]. In the case of Alulight type foam, $[L/2R]_{95th}$ ~ 0.6 [54]. Following this, the theoretically predicted $\sigma_c^{*curvature}$, using expression 6 and considering $f_{curvature}$ for *L/2R* ~ 0.6 [13], has been also plotted in figure 11 (thick black solid line). The line representing the improved model is now between the lines predicted by expressions 4 and 5 and approaches the experimental σ_c^* trends observed, supporting the importance of considering the curvature effect when estimating the collapse strength in 'real' foams. However, the experimental data are still below the theoretical prediction.

Accounting the observed deviations from model predictions and the differences in strength observed, one might think that the different foams analysed could have very different *cell wall curvatures*. However, the high values of curvature required to match the experimental data with the model and the evidence of similar pore structures (figure 6) point to the consideration of an additional feature, i.e. the different cell connectivity.

Figure 12a evaluates the effect of pore connectivity on the mechanical properties by plotting values of σ_c^* versus the corresponding open cell content (C_{open}, measured by pycnometry) in groups of samples of similar relative density, in particular ρ_r ~ 0.18, ρ_r ~ 0.24

and ρ_r ~ 0.31. The figure also includes the trend lines for these experimental points (linear fits) and the theoretical values of $\sigma_c{}^{*curvature}$ according to expression 6 (hollow symbols), which are obviously located at C_{open} = 0.

The results indicate that collapse strength decreases linearly with the open cell content (C_{open}). When extrapolating to C_{open} = 0 the strength values match well with those predicted by expression 6 (hollow symbols in figure 12a). On the other hand, when extrapolating to C_{open} = 100%, the experimental values of σ_c*do not meet the open cell model predictions (expression 4), as it might be expected. This suggests that "closed cell" foams with a regular pore size but with high interconnectivity should not necessary behave as an open cell structures since cell walls are still present in the structure and may have a certain contribution on the global strength of the foam. Obviously, in case or additional defects in the cellular structure, such as significant density inhomogeneities, the collapse strength can end closer to, or even below, the predictions for open cell foams (expression 4), explaining results shown in previous works [2, 3, 4].

In order to clarify whether the contribution of pore connectivity to the strength reduction is independent of sample relative density, the experimental values shown in figure 12a have been normalized by the corresponding strength value at null connectivity (C_{open} = 0, expression 6). The result of this normalization (σ_c* / $\sigma_c{}^{*curvature}$) is shown in figure 12b. It can be observed how the data practically lie on a straight line from 1 to 0.5. This result suggests the possibility of modelling the influence of pore connectivity on collapse strength by simply introducing an additional, new, factor (f_{Copen}) into expression 6. It is possible to observe that, contrary to the known dependence of $f_{curvature}$ with relative density (increases) [12], we can model f_{Copen} as an independent factor.

The further improved model can thus be described as shown in expression 7, where the reduction factor, f_{Copen}, depends on C_{open} as $f_{Copen} = (1- K') C_{open}$, and K' is a coefficient to be determined empirically (in our particular case takes a value of approximately 0.5).

$$\sigma_C^* = \sigma_C^{*CC} f_{curvature} f_{C_{open}} \tag{7}$$

The prediction lines for collapse strength taking into account this K' value and the average values of C_{open} for each type of cooling (table 1, column 3), are plotted in figure 11 together with the experimental data and the three models already commented (expressions 4 to 6). As it can be appreciated, the consideration of this new factor (f_{Copen}), which depends on the experimentally determined open cell content value (C_{open}), allows the proposed model to meet the experimental data with good agreement. This result remarks the importance of considering the pore interconnections at the same level of other types of defects when trying to explain and/or understand the low values and the high scattering in mechanical properties for foams with a similar density [5, 6, 7].

4. Conclusions

Based on the results shown in this work, some important conclusions can be established:

- Increasing the solidification rate during the cooling step can be used as a strategy to control and reduce the size and relative abundance of the pore interconnections inside the cellular structure of metal foams.
- Pycnometry and X-ray tomography have proved their effectiveness when used together for pore connectivity evaluation. Pycnometry enables the evaluation of the open cell content (C_{open}) and X-ray tomography allows the determination of the exact location and size of the pore interconnections.
- It has been observed that pore interconnections tend to be located principally at the central region of the foam where the cooling rate is slower and/or the regions with a

reduced local density. However, if solidification is slow, pore connectivity can also be found in higher fractions near the outer skin.

- It has been found that the enchancement of mechanical properties of the foams when increasing the solidification rate can not be only explained based on the expected refinement of the matrix. Due to the reduction of pore connectivity, increasing the solidification rate also influences the response of the cellular structure, and therefore the global response of the foam (matrix + structure) is much higher.
- The collapse strength values of "real" closed-cell foam samples are located between the theoretical predictions by Gibson and Ashby for open cell and closed cell foams, even when considering the effect of cell wall curvature.
- It has been found that the collapse strength of foams decreases linearly with the pore connectivity grade. This result has allowed to propose a correction factor -f_{Copen}- associated only to the pore connectivity measured by pycnometry (C_{open}).
- The proposed modification of the established model permits more accurate predictions of the collapse strength for closed-cell aluminium foams, accounting for the variability associated with different levels of the pore connectivity induced by different cooling methods post-foaming. This approach is expected to be invaluable in future investigations relating to processing-structure-mechanical property relationships in metal foams.

Acknowledgements

Financial assistance the Spanish Ministry of Science and Innovation and FEDER (MAT2009-14001-C02-01 and MAT2012-34901) is gratefully acknowledged. In addition, the authors are grateful to the Spanish Ministry of Science and Education which supported this investigation with a FPU-doctoral grant Ref-AP-2007-03318 (Jaime Lázaro) and Juan de la

Cierva grant JCI-2011-09775 (Eusebio Solórzano). Authors would also like to thank Alulight Company for having provided the precursor material used in this study.

References

[1] Banhart J (2001) *Manufacture, characterisation and application of cellular metals and metallic foams*. Prog Mater Sci 46(6):559-632

[2] Gibson LJ, Ashby MF (1997) Cellular Solids: Structure and Properties, 2nd edn. Cambridge University Press, Cambridge

[3] Olurin OB, Fleck NA, Ashby MF (2000) Deformation and fracture of aluminium foams. Mater Sci Eng A 291:136-146

[4] Gibson LJ (2000) Mechanical behaviour of metallics foams. Annu Rev Mater Sci 30:191-227

[5] Ramamurty U, Paul A (2004) Variavility in the mechanical properties of a metal foam. Acta Mater 52:869-876

[6] Kennedy AR (2004) Aspects of the reproducibility of mechanical properties in Al based foams. J Mater Sci 39:3085-3088

[7] Nosko M, Simancik F, Florek R (2010) Reproducibility of aluminium foam properties: effect of precursor distribution on the structural anisotropy and the colapse stress and its dispersion. Mater Sci Eng A 527:5900-5908

[8] Banhart J, Baumeister J (1998) Deformation characteristics of metal foams. J Mater Sci 33:1431-1440

[9] Seeliger HW (2002) Manufacture of Aluminum Foam Sandwich (AFS) Components. Adv Eng Mater 4:753-758

[10] McCormack TM, Miller R, Kelser G, Gibson LJ (2001) Failure of sandwich beams with metallic foam cores. Int J Solids Struct 38:4901-4920

[11] Kesler O, Crews LK, Gibson LJ (2003) Creep of sanswich beams with metallic foam cores. Mat Sci Eng A 341:264-272

[12] Simone AE, Gibson LJ (1998) The effect of cell face curvature and corrugations on the stiffness and strength of metallic foams. Acta Mater 46(11):3929-3935

[13] Simone AE, Gibson LJ (1998) Effects of solid distribution on the stiffness and strength of metallic foams. Acta Mater 46(6):2139-2150

[14] Bart-Smith H, Bastawros AF, Mumm DR, Evans AG, Sypeck DJ, Wadley HNG (1998) Compressive deformation and yielding mechanisms in cellular Al alloys determined using X-ray tomography and surface strain mapping. Acta Mater 46(10):3583-3592

[15] Gioux G, McCormack TM, Gibson LJ (2000) Failure of aluminum foams under multiaxial loads. Int J Mech Sci 42:1097-1117

[16] Jeon I, Asahina T (2005) The effect of structural defects on the compressive behavior of closed-cell Al foam. Acta Mater 53:3415-3423

[17] Banhart J, Schmoll C, Neuman U (1998) Light-weight aluminium foam structures for ships. In: Faria L (ed). Proceedings, vol 1. Sociedade Portuguesa de Materials, Lisbon, pp 55-63

[18] Lu TJ, Hess A, Ashby MF (1999) Sound absorption in metallic foams. J Appl Phys 85(11):7528-7539

[19] Lu TJ, Chen F, He D (2000) Sound absorption of cellular metals with semi-open cells. J Acoust Soc Am 108:1697-1709

[20] Wang X, Lu TJ (1999) Optimized acoustic properties of cellular solids. J Acoust Soc Amer 106:756-765

[21] Lazaro J, Solorzano E, Escudero J, de Saja JA, Rodriguez-Perez MA (2012) Applicability of solid solution heat treatments to aluminium foams. Metals 2:508-528

[22] Lu TJ, Stone HA, Ashby MF (1998) Heat transfer in open-cell metal foams. Acta Mater 46:3619-3635

[23] Lu TJ, Chen C (1999) Thermal transport and fire retardance properties of cellular aluminium alloys. Acta Mater 47:1469-1485

[24] McCullough KYG, Fleck NA, Ashby MF (1999) Uniaxial stressstrain behaviour of aluminium foams. Acta Mater 47:2323–2330

[25] Elmouataouakkil A, Salvo L, Maire E, Peix G (2002) 2D and 3D characterization of metal foams using X-ray tomography. Adv Eng Mater 4:803–807

[26] Solorzano E, Rodriguez-Perez MA, de Saja JA (2008) Do we really produce closed cell metallic foams? In: Hirsch J, Skrotzki B, Gottstein G (eds) Proc of the ICAA-11, Wiley-VCH, Weinheim, pp 2200–2205

[27] Yu CJ, Eifert HH, Banhart J, Baumeister J (1998) Metal foaming by a powder metallurgical method: production, properties and applications. J Mater Res Innov 2:181–188

[28] Stanzick H, Wichmann M, Weise J, Helfen L, Baumbach T, Banhart J (2002) Process control in aluminium foam production using real-time x-ray radioscopy. Adv Eng Mater 4(10):814-823

[29] Mukherjee M (2009) Evolution of metal foams during solidification. PhD Dissertation, Tech Univ, Berlin

[30] Mukherjee M, Garcia-Moreno F, Banhart J (2007) Anomalous behaviour of aluminium foams during solidification. Trans Indian Inst Met 60:133–136

[31] Mukherjee M, Garcia-Moreno F, Banhart J (2010) Solidification of aluminium foams. Acta Mater 58:6358–6370

[32] Mukherjee M, Garcia-Moreno F, Banhart J (2010) Defect generation during solidification of aluminium foams. Scr Mater 63:235–238

[33] Lazaro J, Solorzano E, Rodriguez-Perez MA, Garcia-Moreno F (2015) Pore connectivity of aluminium foams: effect of production parameters. J Mater Sci 50(8):3149-3163

[34] Mukherjee M, Ramamurty U, Garcia-Moreno F, Banhart J (2010) The effect of cooling rate on structure and properties of closedcell aluminium foams. Acta Mater 58:5031–5042

[35] Lehmhus D, Banhart J (2003) Properties of heat-treated aluminium foams. Mater Sci Eng A 349:98-110

[36] East J, Maxwell I (1985) Continuous extrusion of metals. US patent No. 4552520

[37] Solorzano E, Reglero JA, Rodriguez-Perez MA, de Saja JA, Rodriguez-Mendez ML (2007) Improvement of the foaming process for 4045 and 6061 aluminium foams by using the Taguchi methodology. J Mater Sci 42:7227–7238

[38] Solorzano E (2008) Aluminium foams: foaming process, structure and properties. PhD Dissertation, Univ Valladolid

[39] ASTM D6226-05 Standard test method for open-cell content of rigid cellular plastics by the air pycnometer

[40] http://www.skyscan.be/home.htm (Last accessed 03-May-2016)

[41] http://www.octopusimaging.eu (Last accessed 03-May-2016)

[42] Brabant L, Vlassenbroeck J et al (2011) Three-dimensional analysis of high-resolution X-ray computed tomography data with Morpho+. Microsc Microanal 17:252–263

[43] ASTM E384-11e1. Standard Test Method for Knoop and Vickers Hardness of Materials.

[44] JIS-H-7902. Method for compressive test of porous metals. Japanese Standards Association.

[45] Garcia-Moreno F, Raffaele N, Banhart J (2008). Optimisation of mould filling during PM metal foaming, in: Stephani G (Ed.). Cellular metals for structural and functional applications: CELLMET 2008. Dresden, 133-138

[46] Helwig HM, Banhart J (2003). Heat distribution during metal foaming, in: Banhart J, Fleck NA, Mortensen A (Eds.). Cellular Metals: Manufacure, Properties and Applications. MIT-Verlag, Berlin, 165-168

[47] Lazaro J, Escudero J, Solorzano E, Rodriguez-Perez MA, de Saja JA (2009) Heat Transport in Closed Cell Aluminum Foams: Application Notes. Adv Eng Mater 11:825-831

[48] Solorzano E, Rodriguez-Perez MA, Reglero JA, de Saja JA (2007) Density gradients in aluminium foams: characterisation by computed tomography and measurements of the effective thermal conductivity. J Mater Sci 42:2557–2564

[49] Shabestari SG, Malekan M (2005) Thermal analysis study of the effect of the cooling rate on the microstructure and solidification parameters of 319 aluminum alloy. Can Metall Quart 44:305-312

[50] Khan S, Ourdjini A, Named QS, Alam Najafabadi MA, Elliott R (1993) Hardness and mechanical property relationships in directionally solidified aluminium-silicon eutectic alloys with different silicon morphologies. J Mater Sci 28:5957-5962

[51] Petch NJ (1953) The cleavage strength of polycrystals. J Iron Steel Inst 174:25-28

[52] Courtney T H (2000) Mechanical behavior of materials, 2nd ed. Boston:McGraw-Hill.

[53] Andrews E, Sanders W, Gibson LJ (1999) Compressive and tensile behaviour of aluminum foams. Mater Sci Eng.A 270:113-124

[54] Sanders W (2002) Mechanical behaviour of closed-cell and hollow sphere metallic foams. PhD Dissertation, MIT

TABLES

Table 1. Results from the analysis of the foams produced under duferent cooling conditions

Cooling type	Solidification rate (K/s)	Open cell content (%)	Nº pore connections (n_i)	Mean interconnection size (μm)	Total Volume (mm^3)	Average Vickers Microhardness	Calculated matrix strength (MPa)
Slow air blowing	0.7 ± 0.2	90.6 ± 5.1	1848	312	13.50	44.1 ± 3.4	147 ± 11
Fast air blowing	1.7 ± 0.5	72.4 ± 6.7	1783	223	7.38	46.3 ± 3.5	154 ± 12
Water quenching	15.0 ± 3.0	25.5 ± 7. 9	653	173	1.87	52.7 ± 3.8	176 ± 13

FIGURE CAPTIONS

Fig. 1. Schematic of the system used to measure the temperature evolution in the foams during the cooling step.

Fig. 2. Variation of temperature at the centre of three foams (p ~ 0.76 ± 0.01) during the different cooling processes. Foaming temperature of 650ºC (furnace/mould temperature).

Fig. 3. Open cell content versus foam porosity for different cooling methods.

Fig. 4. X-ray tomography slices at the centre of three representative foams for the different solidification conditions evaluated (p ~ 0.76) (a) Slow air blowing (b) Fast air blowing (c) Water quenching.

Fig. 5. Vertical porosity distribution, from top to bottom, for the three representative foams shown in figure 4. p_{air_1bar} = 0.76 ± 0.02; p_{air_6bar} = 0.74 ± 0.02; p_{water} = 0.75 ± 0.03.

Fig. 6. (a) 3D pore size distributions and (b) sphericity histograms for the foams shown in figure 4.

Fig. 7. 3D distribution of interconnections inside two foams. (a) Specimen with high open cell content (solidified using air), (b) Specimen with low open cell content (solidified by water quenching).

Fig. 8. Interconnection size distributions.

Fig. 9. Microhardness profiles, at the mid-height, for foams produced under different cooling conditions. Dashed lines show the average trend.

Fig. 10. Compressive stress-strain response for three representative foams of similar structural characteristics. (p = 0.77 ± 0.01; Φ~1.30 ± 0.02 mm), but produced under different cooling conditions (figure 4).

Fig. 11. Normalized collapse strength as a function of relative density. Lines correspond to the predictions from theoretical models (eq. 4 and 5), including the effect of curvature (eq. 6), and the effect of pore connectivity (eq. 7).

Fig. 12. (a) Variation of σ_c* with C_{open}. (b) Variation of f_{Copen} with C_{open} (to be used in expression 7).

Fig. 1

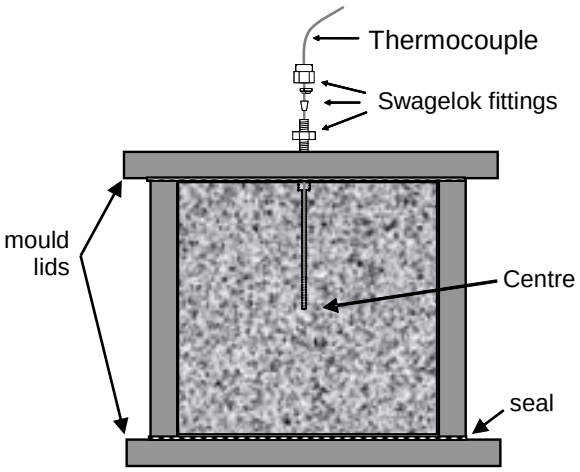

Fig. 2

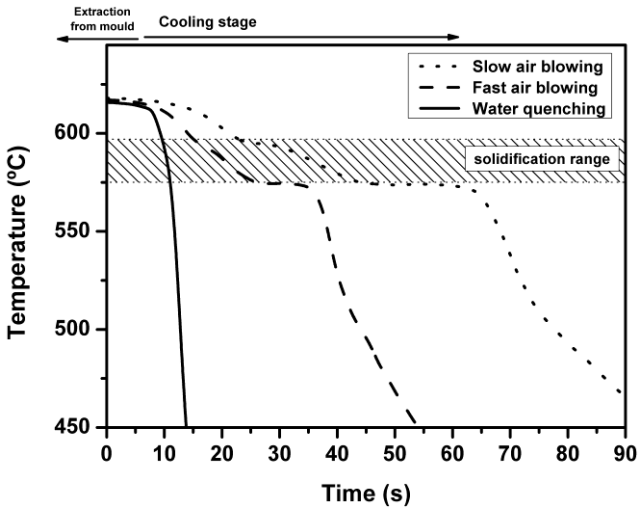

Fig. 3

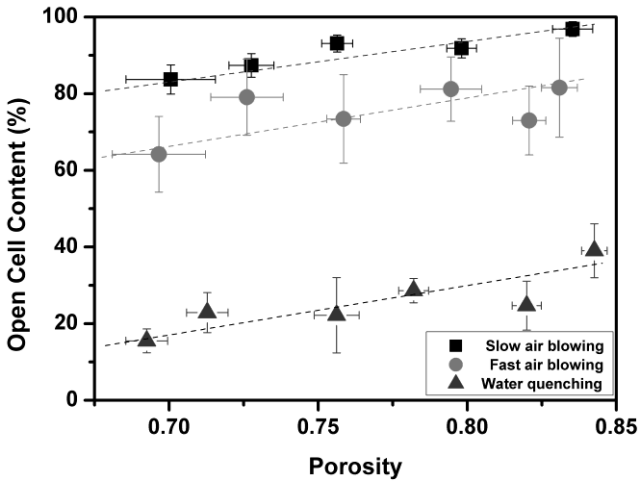

Fig. 4

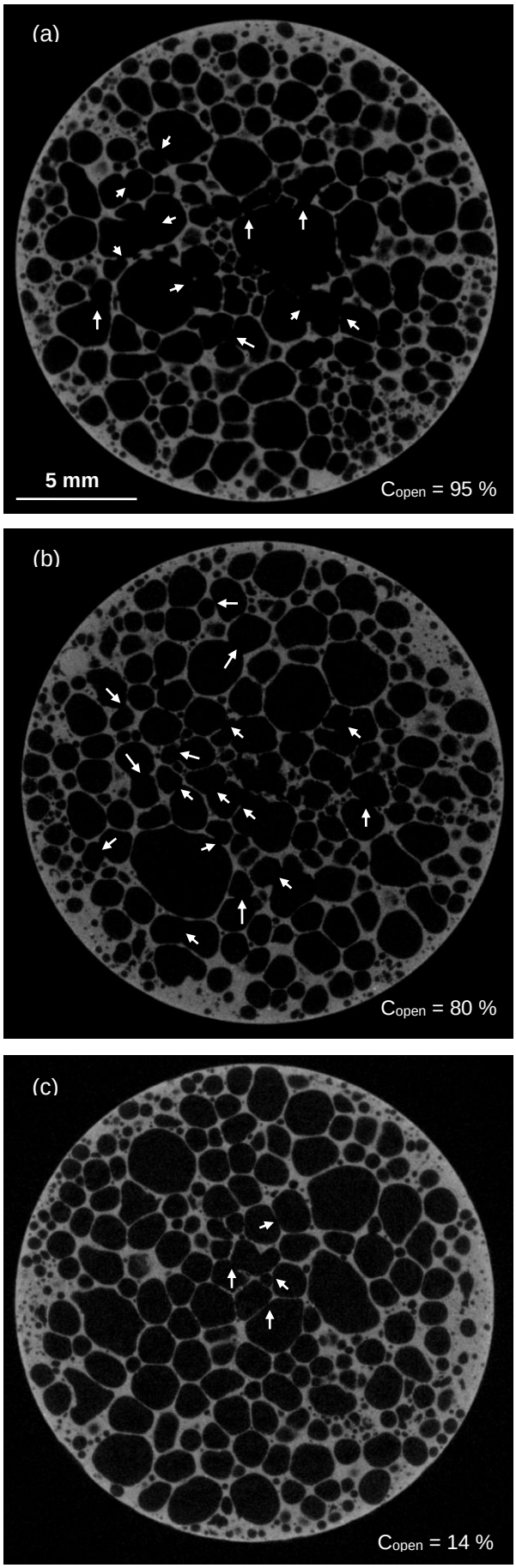

Fig. 5

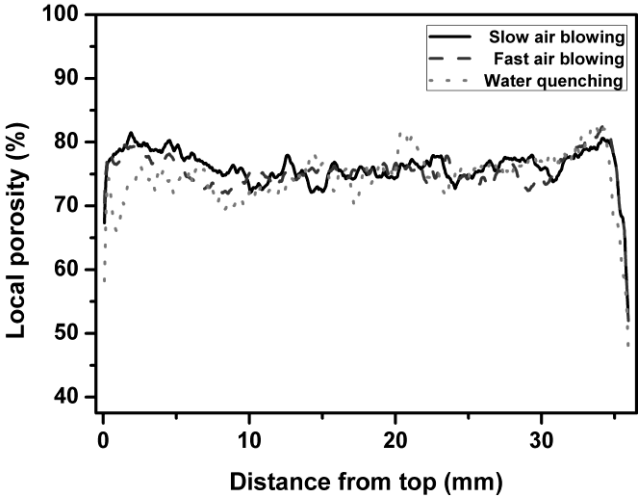
Slow air blowing
Fast air blowing
Water quenching
Local porosity (%)
Distance from top (mm)

Fig. 6

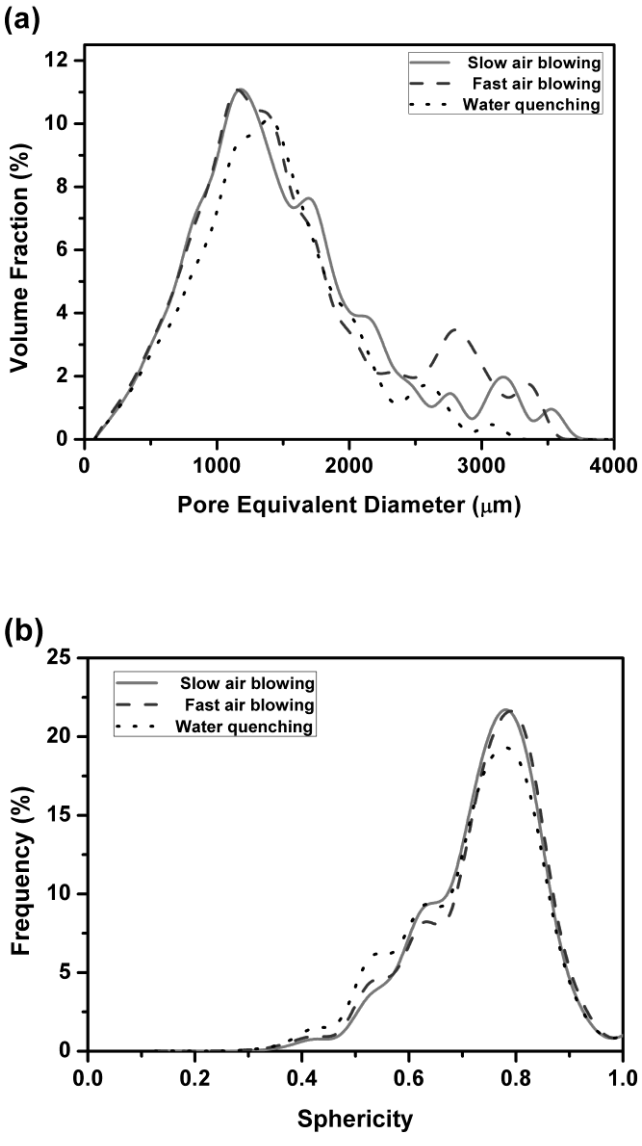
(a)
Slow air blowing
Fast air blowing
Water quenching
Volume Fraction (%)
Pore Equivalent Diameter (μm)
(b)
Slow air blowing
Fast air blowing
Water quenching
Frequency (%)
Sphericity

Fig. 7

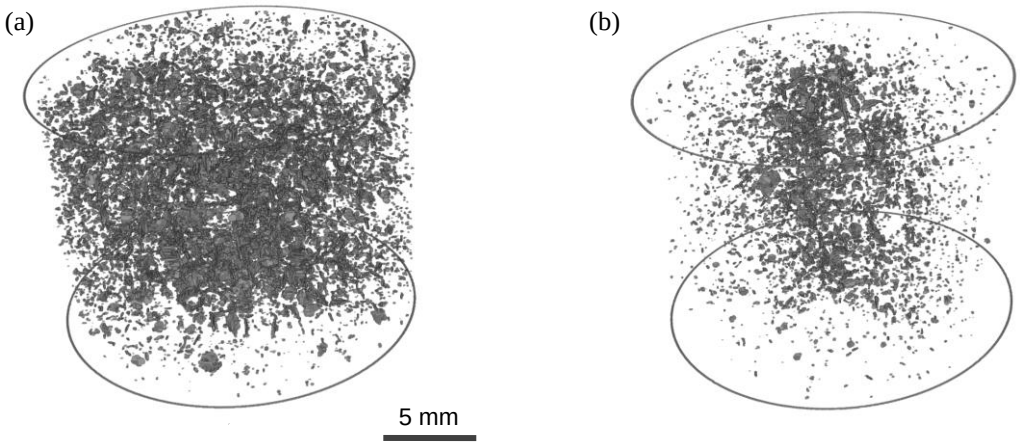

Fig. 8

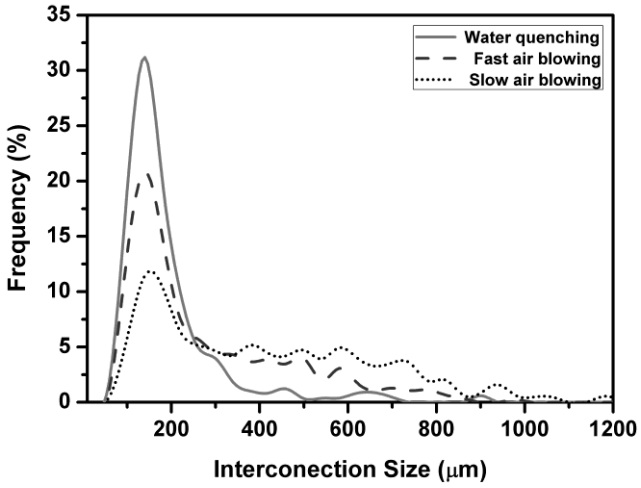

Fig. 9

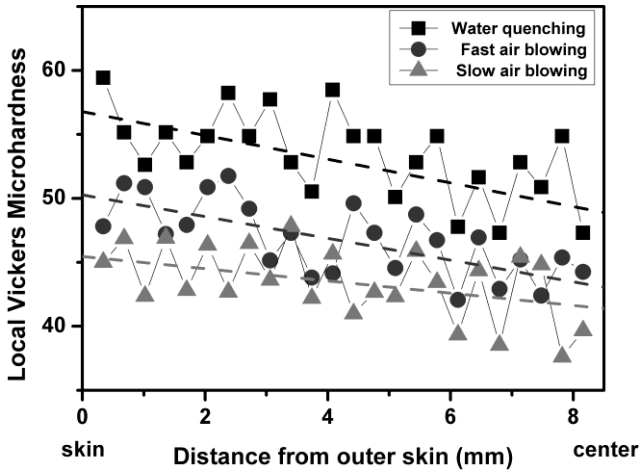

Fig. 10

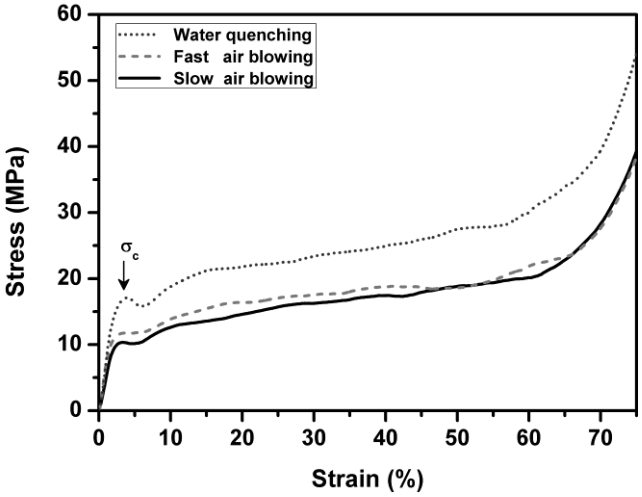
Water quenching
Fast air blowing
Slow air blowing
σc
Stress (MPa)
Strain (%)
0
10
20
30
40
50
60
70

Fig. 11

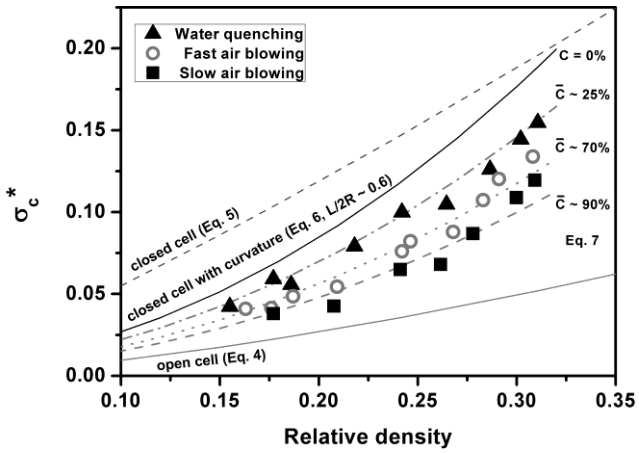
Water quenching
Fast air blowing
Slow air blowing
C = 0%
C̄ ~ 25%
C̄ ~ 70%
C̄ ~ 90%
Eq. 7
closed cell (Eq. 5)
closed cell with curvature (Eq. 6, L/2R ~ 0.6)
open cell (Eq. 4)
σc*
Relative density
0.00
0.05
0.10
0.15
0.20
0.10
0.15
0.20
0.25
0.30
0.35

Fig. 12

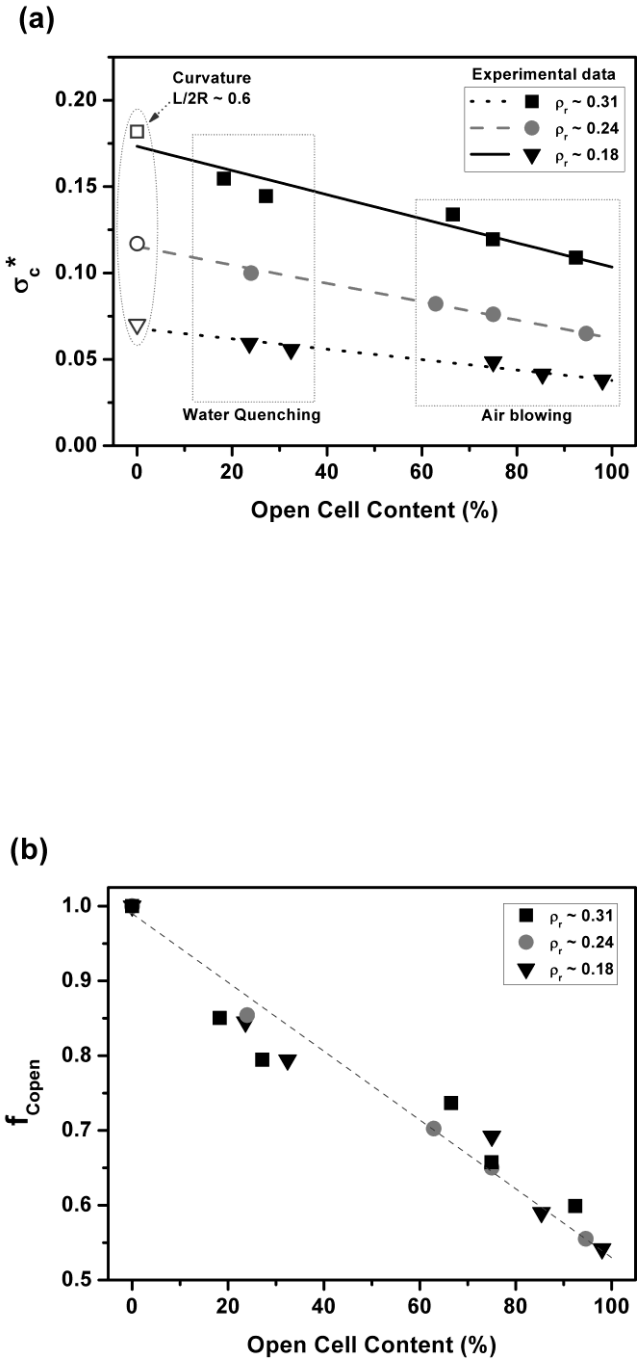
(a)
Curvature
L/2R ~ 0.6
Experimental data
ρr ~ 0.31
ρr ~ 0.24
ρr ~ 0.18
σc*
0.20
0.15
0.10
0.05
0.00
Water Quenching
Air blowing
0
20
40
60
80
100
Open Cell Content (%)
(b)
ρr ~ 0.31
ρr ~ 0.24
ρr ~ 0.18
fCopen
1.0
0.9
0.8
0.7
0.6
0.5
0
20
40
60
80
100
Open Cell Content (%)